# Building patterns by traveling dipoles and vortices in two-dimensional periodic dissipative media

Valentin Besse, Hervé Leblond, Dumitru Mihalache, Boris Malomed

Optics Communications 332 (2014) 279–291

Contents lists available at ScienceDirect

Optics Communications

journal homepage: www.elsevier.com/locate/optcom

# Building patterns by traveling dipoles and vortices in two-dimensional periodic dissipative media

V. Besse [a,*], H. Leblond [a], D. Mihalache [a,b,c], B.A. Malomed [d]

[a] LUNAM Université, Université d'Angers, Laboratoire de Photonique d'Angers, EA 4464, 2 Boulevard Lavoisier, 49000 Angers, France
[b] Horia Hulubei National Institute for Physics and Nuclear Engineering, 30 Reactorului, Magurele-Bucharest 077125, Romania
[c] Academy of Romanian Scientists, 54 Splaiul Independentei, 050094 Bucharest, Romania
[d] Department of Physical Electronics, School of Electrical Engineering, Faculty of Engineering, Tel Aviv University, Tel Aviv 69978, Israel

ARTICLE INFO

*Article history:*
Received 6 March 2014
Received in revised form
18 June 2014
Accepted 7 July 2014
Available online 18 July 2014

*Keywords:*
Pattern formation
Dissipative soliton
Spatial soliton
Vortex
Complex Ginzburg–Landau equation
Nonlinear dynamics

ABSTRACT

We analyze pattern-formation scenarios in the two-dimensional (2D) complex Ginzburg–Landau (CGL) equation with the cubic–quintic (CQ) nonlinearity and a cellular potential. The equation models laser cavities with built-in gratings, which stabilize 2D patterns. The pattern-building process is initiated by kicking a compound mode, in the form of a dipole, quadrupole, or vortex which is composed of four local peaks. The hopping motion of the kicked mode through the cellular structure leads to the generation of various extended patterns pinned by the structure. In the ring-shaped system, the persisting freely moving dipole hits the stationary pattern from the opposite side, giving rise to several dynamical regimes, including periodic elastic collisions, i.e., persistent cycles of elastic collisions between the moving and quiescent dissipative solitons, and transient regimes featuring several collisions which end up by absorption of one soliton by the other. Still another noteworthy result is the transformation of a strongly kicked unstable vortex into a stably moving four-peaked cluster.



## 1. Introduction

The fundamental principle behind the creation of dissipative solitons is that their stability relies upon the simultaneous balance of conservative and dissipative ingredients in the underlying system [1]. These are the diffraction and self-focusing nonlinearity in the conservative part of the system, and the linear and nonlinear loss and gain terms in the dissipative part. Well-known physical realizations of such systems are offered by lasing [2,3] and plasmonic [4] cavities, the respective models being based on the complex Ginzburg–Landau (CGL) equations with the cubic–quintic (CQ) set of gain and loss terms, combined with the background linear loss [3]. This combination is well known to maintain stable localized modes [5]. The CGL equations constitute a generic class of dissipative pattern-formation models [6], which find many other applications, including bosonic condensates of quasi-particles in solid-state media [7], reaction–diffusion systems [8], and superconductivity [9].

Originally, the CGL equation of the CQ type was introduced [5] as a model for the creation of stable two-dimensional (2D) localized modes. Following this work, similar models were derived or proposed as phenomenological ones in various settings. Many 1D and 2D localized states, i.e., dissipative solitons, have been found as solutions of such equations [10–15].

An essential ingredient of advanced laser cavities is a transverse periodic grating, which can be fabricated by means of available technologies [16]. In addition to the permanent gratings, virtual photonic lattices may be induced in photorefractive crystals as interference patterns by pairs of pump beams with the ordinary polarization, which illuminate the crystal along the axes $x$ and $y$, while the probe beam with the extraordinary polarization is launched along $z$ [17]. A 2D cavity model with the grating was introduced in Ref. [18]. It is based on the CQ-CGL equation including the cellular (lattice) potential, which represents the grating. In fact, the laser cavity equipped with the grating may be considered as a photonic crystal built in the active medium. Periodic potentials also occur in models of passive optical systems, which are driven by external beams and operate in the temporal domain, unlike the active systems which act in the spatial domain [19–21].

Localized vortices, alias vortex solitons, are an important species of self-trapped modes in 2D settings. In uniform media, dissipative vortex solitons cannot be stable without the presence of a diffusion term, in the framework of the CGL equation (see, e.g., Ref. [12]). However, this term is absent in models of waveguiding

* Corresponding author.
*E-mail addresses:* valentin.besse@univ-angers.fr, valentin.besse@hotmail.fr (V. Besse).

http://dx.doi.org/10.1016/j.optcom.2014.07.029
0030-4018/

systems (it may sometimes be present in temporal-domain optical models [22]). Compound vortices, built as complexes of four peaks pinned to the lattice potential, may be stable in models including the grating in the absence of the diffusion [18]. Using this possibility, stable 2D [23] and 3D [24] vortical solitons have been found in the framework of CGL equations including trapping potentials.

In a majority of previous works, the studies of various 2D localized patterns have been focused on their stabilization by means of the lattice potentials. Another relevant issue is the mobility of 2D dissipative solitons in the presence of the underlying lattice (dissipative solitons may move without friction only if the diffusion term is absent, therefore the mobility is a relevant issue for the diffusion-free models of laser cavities). Localized modes can be set in motion by the application of a kick to them, which, in the context of the laser-cavity models, implies launching a tilted beam into the system. Recently, the mobility of kicked 2D fundamental solitons in the CQ-CGL equation with the cellular potential was studied in Ref. [25]. It has been demonstrated that the kicked soliton, hopping through the periodic structure, leaves in its wake various patterns in the form of single- or multi-peak states trapped by the periodic potential. In the case of periodic boundary conditions (b.c.), which correspond to an annular system, the free soliton completes the round trip and hits the pattern that it has originally created. Depending on parameters, the free soliton may be absorbed by the pinned mode (immediately, or after several – up to five – cycles of quasi-elastic collisions), or the result may be a regime of periodic elastic collisions, which features periodic cycles of passage of the moving soliton through the quiescent one.

A natural extension of the analysis performed in Ref. [25] is the study of the mobility of kicked soliton complexes, such as dipoles, quadrupoles, and compound vortices, and various scenarios of the dynamical pattern formation initiated by such moving complex modes, in the framework of the 2D CQ-CGL equation with the lattice potential. This is the subject of the present work. In fact, such configurations are truly two-dimensional ones, while the dynamical regimes for kicked fundamental solitons, studied in Ref. [25], actually represent quasi-1D settings. The model is formulated in Section 2, which is followed by the presentation of systematic numerical results for dipoles, quadrupoles, and vortices of two types, onsite- and offsite-centered ones (alias "rhombuses" and "squares") in Sections 3, 4, and 5, respectively. The paper is concluded in Section 6.

An essential finding is that the interaction of a freely moving dipole with pinned patterns, originally created by the same kicked dipole, gives rise to new outcomes under the periodic b.c. In particular, the quiescent dipole can be absorbed (cleared) by the moving one, which may have obvious applications to the design of all-optical data-processing schemes, where one may need to install or remove a blocking soliton. Also noteworthy is the transformation of an unstable vortex by a strong kick into a stable moving four-soliton cluster.

## 2. The cubic–quintic complex Ginzburg–Landau model with the cellular potential

The CQ-CGL equation with a periodic potential is written as

$$\frac{\partial u}{\partial Z}=\left[-\delta+\frac{i}{2}\nabla_{\perp}^{2}+(i+\epsilon)|u|^{2}-(i\nu+\mu)|u|^{4}+iV(X,Y)\right]u. \tag{1}$$

It describes the evolution of the amplitude of electromagnetic field $u(X,Y,Z)$ along propagation direction $Z$, with transverse Laplacian $\nabla_{\perp}^{2}=\partial^{2}/\partial X^{2}+\partial/\partial Y^{2}$. Parameter $\delta$ is the linear-loss coefficient, $\epsilon$ is the cubic gain, $\mu$ the quintic loss, and $\nu$ the quintic self-defocusing coefficient (it accounts for the saturation of the Kerr effect if $\nu>0$). The 2D periodic potential with amplitude $V_0$ is taken in the usual form, $V(X,Y)=V_0[\cos(2X)+\cos(2Y)]$, where the normalization of the field and coordinates is chosen so as to make the normalized period equal to $\pi$, which is always possible. The total power of the field is also defined as usual:

$$P=\iint|u(X,Y)|^{2}\,dX\,dY. \tag{2}$$

We solved CGL equation (1) by means of the fourth-order Runge–Kutta algorithm in the $Z$-direction, and five-point finite-difference scheme for the computation of the transverse Laplacian $\nabla_{\perp}^{2}$. Periodic boundary conditions (b.c.) were used for the study of kicked dipoles and quadrupoles, and absorbing b.c. for kicked vortices. In the latter case, the absorbing b.c. are implemented by adding a surrounding linear-absorption strip to the computation box. The absorption coefficient varies quadratically with $X$ and $Y$ from zero at the internal border of the strip to a value large enough to induce complete absorption of any outgoing pulse, at its external border. This smooth variation, if the width of the strip is not too small, allows one to suppress any reflection from the absorption strip.

Values of coefficients chosen for numerical simulations are $\delta=0.4$, $\epsilon=1.85$, $\mu=1$, $\nu=0.1$, and $V_0=-1$. This choice corresponds to a set of parameters for which the initial static configurations for the dipoles, quadrupoles, and vortices are stable (in-phase bound states of two dissipative solitons are also possible, but, unlike the dipoles, with the phase shift of $\pi$ between the bound solitons, they are unstable). The kick is applied to them in the usual way, by adding the linear phase profile to the initial field:

$$u_0(X,Y)\to u_0(X,Y)\exp(i\mathbf{k}_0\cdot\mathbf{r}), \tag{3}$$

where $\mathbf{r}\equiv\{X,Y\}$. The key parameters are length $k_0$ of kick vector $\mathbf{k}_0$, and angle $\theta$ which it makes with the $X$-axis:

$$\mathbf{k}_0=(k_0\cos\theta,k_0\sin\theta). \tag{4}$$

In the laser setup the kick corresponds to a small deviation of the propagation direction of the beam from the $Z$-axis. If $K_0$ is the full wave number and $\varphi$ is the deviation angle, the length of the transverse wave vector in physical units is $K_0\sin\varphi$, which corresponds to $k_0$ in the normalized form. Below, we investigate the influence of kick parameters $k_0$ and $\theta$, defined as per Eq. (4), on a variety of multi-soliton complexes, which are created by moving dipoles, quadrupoles, or vortices (of both onsite- and offsite-centered types) in the 2D CGL medium with the cellular potential.

## 3. The pattern formation by kicked dipoles

### 3.1. Generation of multi-dipole patterns by a dipole moving in the transverse direction

In this section we consider the simplest soliton complex in the form of a stable vertical dipole, which consists of a pair of solitons aligned along the $Y$-axis and mutually locked with phase difference $\pi$, which is shown in Fig. 1. The same color code as in Fig. 1 (a) is used in all figures showing amplitude distributions throughout the paper. First, the dipole is set in motion by the application of the kick in the horizontal ($X$) direction (i.e., transverse to the dipole's axis), as per Eqs. (3) and (4) with $\theta=0$.

As shown in Fig. 2, the moving dipole multiplies into a set of secondary ones, similar to the outcome of the evolution of the kicked fundamental soliton [25]. Each newly created dipole features the fixed phase shift $\pi$ between two constituent solitons, and the entire pattern, established as the result of the evolution, is robust. The particular configuration displayed in Fig. 2 is a chain of five trapped dipoles, and a free one, which has wrapped up the motion and reappears from the left edge, moving to the right, due

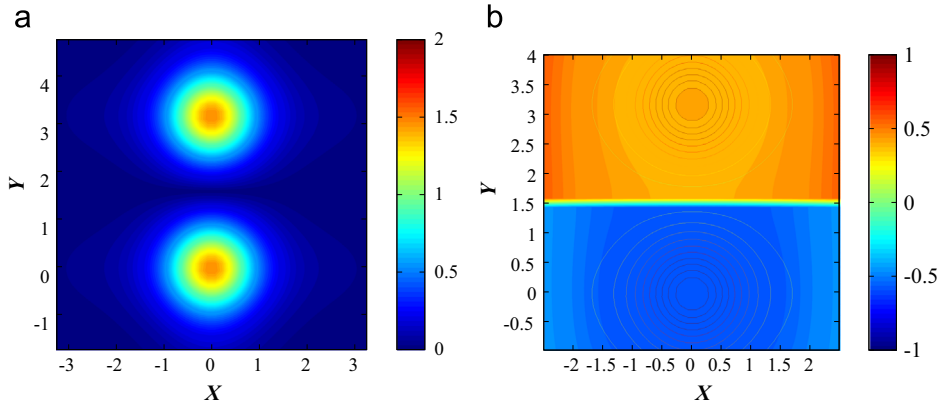


**Fig. 1.** The distribution of the amplitude (a) and phase (in units of $\pi$) (b) in the stable quiescent dipole mode.

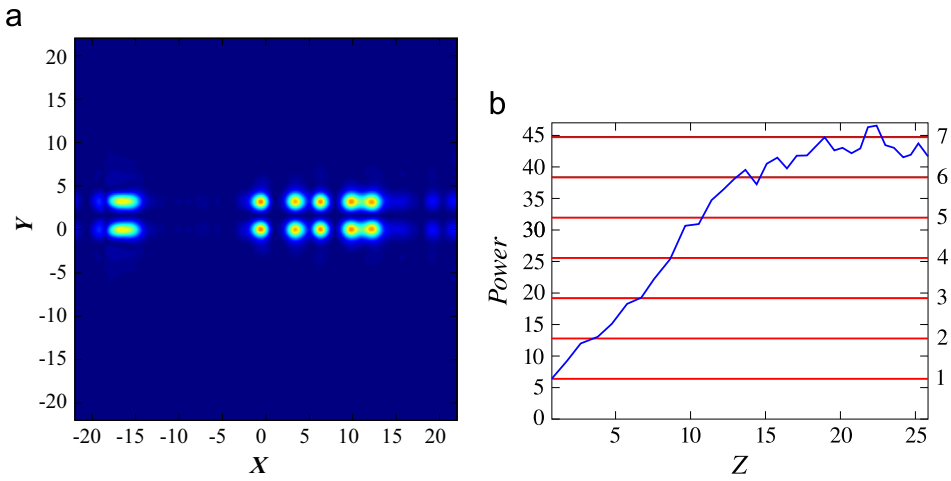


**Fig. 2.** (a) Field $|u(X,Y)|$ produced by the horizontally kicked (with $\theta=0$) vertical dipole at $Z$=22.410, for $k_0=1.665$. In this panel, the leftmost dipole is moving to the right. The color code is the same as in Fig. 1(a). (b) The evolution of the pattern produced by the horizontally kicked dipole, shown in terms of the total power of the field as a function of propagation distance $Z$. The set of horizontal red lines shows power levels corresponding to different numbers ($n$) of quiescent dipoles. (For interpretation of the references to color in this figure caption, the reader is referred to the web version of this paper.)

to the periodic b.c. Then, the free dipole will hit the pinned chain, and will be absorbed by it, yielding a pattern built of five quiescent dipoles. Immediately after the collision, the pattern features intrinsic oscillations, which are gradually damped.

The snapshot shown in Fig. 2 corroborates an inference made from the analysis of numerical results: the largest number of the dipoles generated by the initially kicked one is six, including one moving dipole and five identical quiescent ones. It is worthy to note that, as seen in Fig. 2(b), in this case the total power (2) of the finally established set of six dipoles is close to the net power corresponding to *seven* quiescent ones, which is explained by the observation that the power of the stably moving dipole is, approximately, twice that of its quiescent counterpart.

To study the outcome of this dynamical pattern-formation scenario in a systematic form, we monitored the number of output solitons as a function of the kick's strength, $k_0$. These results are summarized in Fig. 3, which provides an adequate overall characterization of the interactions, including a potential possibility to use these interactions for the design of data-processing setups.

Below the threshold value of the kick's strength, whose numerically found value is

$$k_0^{(\mathrm{thr})}(\theta=0)\approx 1.651, \tag{5}$$

the kicked dipole exhibits damped oscillations, remaining trapped near a local minimum of the cellular potential. Then, as seen in

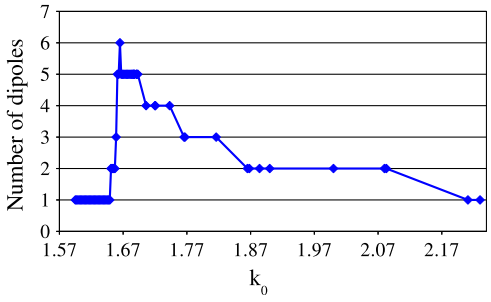


**Fig. 3.** The number of dipoles in the final configuration versus the kick strength, $k_0$, applied to the vertical dipole in the horizontal direction.

Fig. 3, the number of dipoles initially increases steeply with $k_0$, reaching (as mentioned above) a maximum of six at $k_0=1.665$. It is worthy to mention that this value is different from those, ranging in interval $k_0\in[1.6927, 1.6942]$ in which the maximum number of secondary solitons is reached in the case when the kick is applied to a fundamental soliton [25]. This observation suggests that building the structures by the kicked dipole does not merely reduce to the earlier studied regime of the pattern formation by the individual solitons forming the dipole. With the further increase of $k_0$, the number of solitons in the output decreases by increasing broad steps.

### 3.2. Dynamical regimes initiated by the longitudinal kick applied to the dipole

For the sake of the completeness of the description of the 2D system, we have also simulated essentially quasi-1D dynamical regimes initiated by the motion of the dipole kicked at angle of $\theta=\pi/2$, i.e., in the longitudinal direction, see Eq. (4). This setting implies the possibility to generate not only new dipoles but also fundamental solitons. It was found that the minimum value of the kick which is necessary to set the dipole in motion is smaller in this case than the one given by Eq. (5):

$$k_0^{(\mathrm{thr})}(\theta=\pi/2)\approx 1.303. \tag{6}$$

The results obtained for this configuration are summarized in Table 1. Above the threshold value (6), additional moving solitons are created: one at $k_0\in[1.304,1.875]$ and two in a narrow interval $k_0\in[1.880,1.885]$. Then, for $k_0\in[1.89,2.015]$, a new moving dipole appears, which, as well as the original one, is oriented along the direction of the motion, and accompanied by two moving solitons. For $k_0\in[2.02,2.17]$, we have one moving soliton less, and at $k_0\in[2.175,2.255]$ the original dipole disappears in the course of the propagation, thus leaving one moving dipole and two moving solitons in the system. At $k_0\in[2.26,2.36]$, we observe the same pattern as for $k_0\in[2.02,2.17]$ (two dipoles and one moving soliton). Then, for $k_0\in[2.365,2.46]$, the dipole splits into two traveling solitons, with the upper one leaving a pinned soliton at the site which it originally occupied. At higher values of the kick's strength, the same pattern appears, except that the solitons do not leave anything behind them, just traveling through the lattice.

**Table 1**
The number of dipoles and fundamental solitons in the established pattern versus the kick's strength $k_0$ directed along the dipole's axis ($\theta=\pi/2$). In the right column, a newly emerging dipole (if any) is counted as two solitons.

| Behavior pattern | Range of $k_0$ | Number of new solitons along the $Y$-direction |
|---|---|---|
| 1 Dipole | $k_0\in[0,1.303]$ | 0 |
| 1 Dipole and 1 moving soliton | $k_0\in[1.304,1.875]$ | 1 |
| 1 Dipole and 2 moving solitons | $k_0\in[1.88,1.885]$ | 2 |
| 2 Dipoles and 2 moving solitons | $k_0\in[1.89,2.015]$ | 4 |
| 2 Dipoles and 1 moving soliton | $k_0\in[2.02,2.17]$ | 3 |
| 1 Dipole and 2 moving solitons | $k_0\in[2.175,2.255]$ | 2 |
| 2 Dipoles and 1 moving soliton | $k_0\in[2.26,2.36]$ | 3 |
| 1 Pinned and 2 moving solitons | $k_0\in[2.365,2.46]$ | 1 |
| 2 Moving solitons | $k_0\in[2.465,\infty)$ | 0 |

### 3.3. Collision scenarios for moving dipoles in the system with periodic b.c.

The above consideration was performed for a long system, before the collision of the freely moving dipole with the static pattern left in its wake, which should take place in the case of periodic b.c. In the application to laser-cavity settings, the periodic b.c. in the direction of $X$ are relevant, corresponding to the cavity with the annular shape of its cross section. The study of dynamical pattern-formation scenarios with the periodic b.c. is also interesting in terms of the general analysis of models based on the CGL equation [25].

Thus, under the periodic b.c., the freely moving dipole observed in Fig. 2 will complete the round trip and will hit the trapped chain of quiescent dipoles. Results of extensive simulations of this setting are summarized in the list of three different outcomes of the collisions, which feature persistent or transient dynamics (all the regimes were observed for $\theta=0$, i.e., the transversely kicked dipole):

- The regime of the periodic elastic collisions, corresponding to the periodically recurring passage of the moving dipole through the quiescent one, see Fig. 4. This outcome takes place for $k_0\in[1.865,1.868]$. Note that, according to Fig. 3, in this region the pattern left in the wake of the kicked dipole indeed amounts to another single quiescent dipole.
- The transient regime, which features several quasi-elastic collisions, before the moving dipole is eventually absorbed by the pinned pattern, which is a bound complex of two dipoles, see Fig. 5. This transient regime occurs around $k_0=1.816$, in which case Fig. 4 confirms that the moving dipole leaves a set of two additional dipoles in its wake.
- The regime of "clearing the obstacle", opposite to the previous one, which features several elastic collisions, before the pinned dipole is absorbed by the moving one, see Fig. 6. This happens for $k_0\in[1.884,1.9]$ and around $k_0=2.083$ (in this region, Fig. 3 confirms that the moving dipole creates, originally, a single quiescent one).

In other cases, the freely moving dipole is absorbed by the quiescent pattern as a result of the first collision.

It is relevant to stress that, while the first two above-mentioned regimes have been reported in Ref. [25] for the motion of kicked fundamental solitons, the third regime (clearing the obstacle) is a new one, which was not found for the fundamental solitons. Another characteristic feature of the latter regime is that it

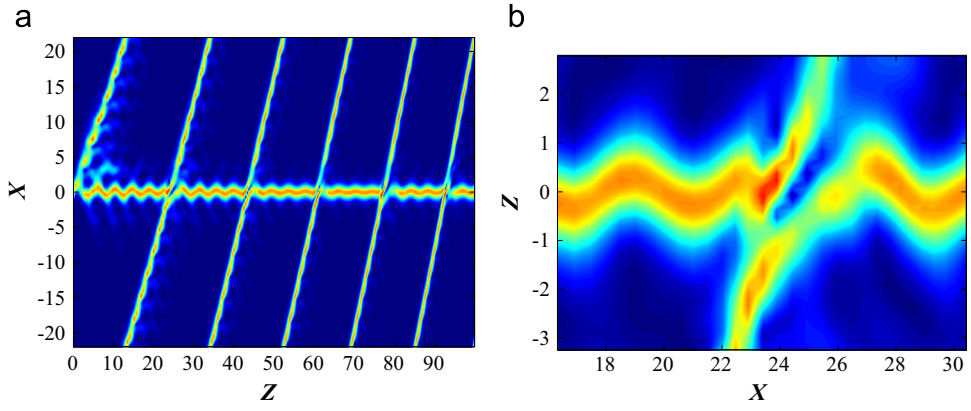


**Fig. 4.** (a) The cross section of field $|u(X,Y,Z)|$ at $Y=0$, in the plane of $(X,Z)$, for $k_0=1.865$. This is an example of the scenario of the periodic elastic collisions, when the moving dipole repeats elastic collisions with the quiescent one. (b) The close-up of the elastic collision. The color code is the same as in Fig. 1(a).

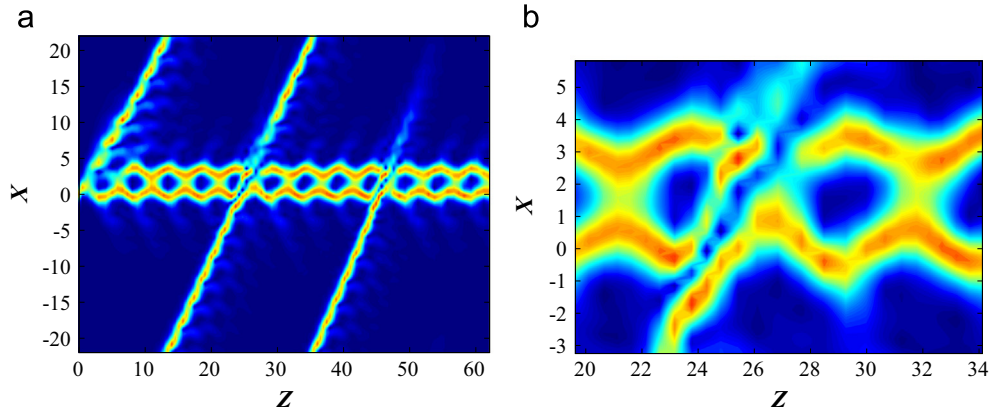


**Fig. 5.** (a) The cross section of field $|u(X,Y,Z)|$ at $Y=0$, in the plane of $(X,Z)$, for $k_0=1.816$. This is an example of the transient regime, when the moving dipole is absorbed by the pair of trapped ones after several quasi-elastic collisions. (b) The close-up of the absorptive collision. The color code is the same as in Fig. 1(a).

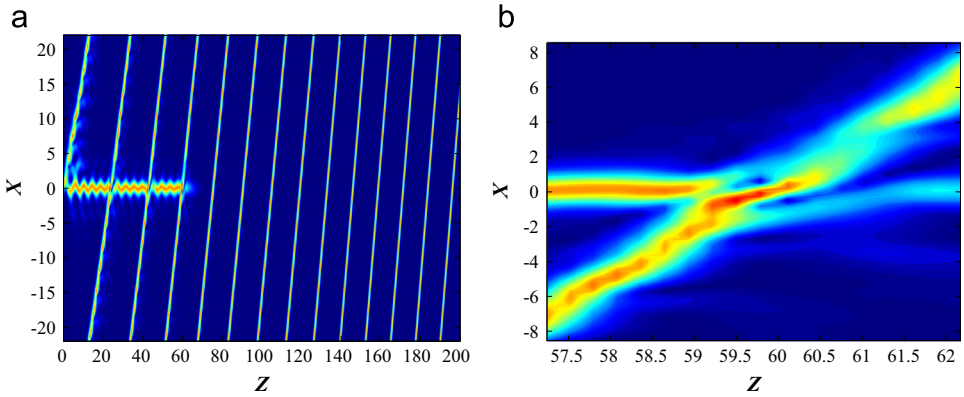


**Fig. 6.** (a) The cross section of field $|u(X,Y,Z)|$ at $Y=0$, in the plane of $(X,Z)$, for $k_0=1.884$. This is an example of "clearing the obstacle", when the moving dipole absorbs the stationary one, after several collisions with it. (b) The close-up of the absorptive collision. The color code is the same as in Fig. 1(a).

eventually leads to the splitting of the surviving single dipole into unbound fundamental solitons, as shown in Fig. 7(a). To analyze the splitting, we have identified position $\{X_c, Y_c\}$ of the field maximum in each soliton (its center), and values of phases at these points (mod $2\pi$), as functions of evolution variable $Z$. As a result, it has been found that the splitting of the dipole and the loss of the phase correlation between the splinters start in a "latent form" at $Z\approx 102.8$, and become explicit at $Z\simeq 112.5$, see Fig. 7(c) and (d). The two splinter solitons get completely separated at $Z\simeq 115$. The splitting also leads to the appearance of the velocity difference between the solitons (the velocity is defined as $dX_c/dZ$), as seen in Fig. 7(b).

## 4. The pattern formation by kicked quadrupoles

A quadrupole is composed of four soliton-like power peaks, which are mutually locked with phase difference $\pi$ between adjacent ones, see an example of the offsite-centered (alias "square-shaped") quadrupole in Fig. 8. Although this mode carries no vorticity, simulations demonstrate that it is a very robust one. We here aim to investigate dynamical regimes initiated by the application of the horizontal kick (3) to the quadrupole.

The quadrupole is set in motion by the kick whose strength exceeds the respective threshold:

$$k_0^{(\mathrm{thr})}(\mathrm{quadr})=1.28, \tag{7}$$

cf. Eqs. (5) and (6). The horizontal motion of the kicked quadrupole splits it into two vertical dipoles, and generates a set of additional vertically arranged quiescent *soliton pairs*, with a phase shift of $\pi/2$ between them. The dependence of the total number of solitons in the eventually established pattern on the kick's strength, $k_0$, is shown in Fig. 9. Because these simulations were subject to the periodic b.c., the free dipole completes the round trip to collide with the quiescent pattern. The number of solitons was counted just before this collision. In the case where there is no motion in the system (no free dipole emerges), the count of the number of solitons is straightforward.

The result is quite different from that reported in the previous section for the pattern formation by the kicked dipole, cf. Fig. 3. Above the threshold value (7), the number of fundamental solitons in the emergent pattern increases and remains constant in a wide interval of values of $k_0$, *viz.*, six solitons for $k_0\in[1.28,1.87]$. Then, the number of the solitons increases to its maximum, which is 14 at $k_0\in[1.89,1.893]$, $k_0=1.91$ and $k_0\in[1.935,1.96]$. Note that the increase is not monotonous. For example, 12 solitons are generated at $k_0=[1.885,1.887]$ and $k_0=[1.895,1.9]$. Subsequently, in the interval of $k_0\in[1.9125,2.338]$, the soliton number varies between 8 and 16. The largest number of solitons, 18, is reached at $k_0=2.339$. Then, the soliton number drops to 6, and this value remains constant over a relatively broad interval, $k_0\in[2.373, 2.475]$. At still larger values of $k_0$, no additional solitons are generated by the initially moving quadrupole, which in this case again splits into two dipoles.

At $k_0=2.339$, the simulations generate a set of 18 solitons (the largest number, as said above). At first, two moving dipoles are actually produced by the splitting of the original quadrupole, see Fig. 10(a). The faster dipole [whose trajectory is characterized by a larger slope (velocity), $dX_c/dZ$] moves without creating new solitons, while the slower one creates several of them, namely

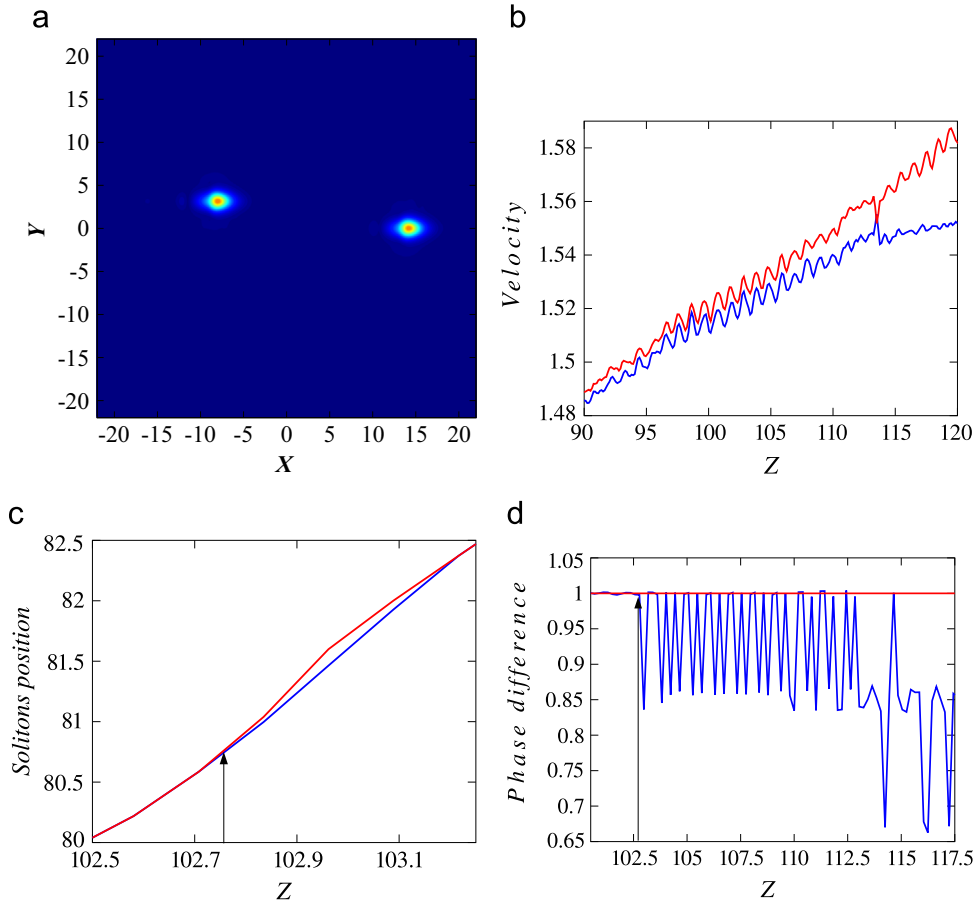


**Fig. 7.** Illustration of the splitting of the single surviving dipole into uncorrelated fundamental solitons, which follows "clearing the obstacle", after the absorption of the quiescent dipole by the moving one, at $k_0 = 1.884$. (a) Field $|u(X, Y)|$ at $Z = 199.965$. The color code is the same as in Fig. 1(a). (b, c) Velocities and positions of both solitons as functions of $Z$. (d) The phase difference between the solitons versus $Z$, in units of $\pi$, the red horizontal line corresponding to the phase difference equal to $\pi$. The arrows in (c) and (d) indicate onset of the process which eventually leads to the loss of the phase coherence and separation of the two solitons. (For interpretation of the references to color in this figure caption, the reader is referred to the web version of this paper.)

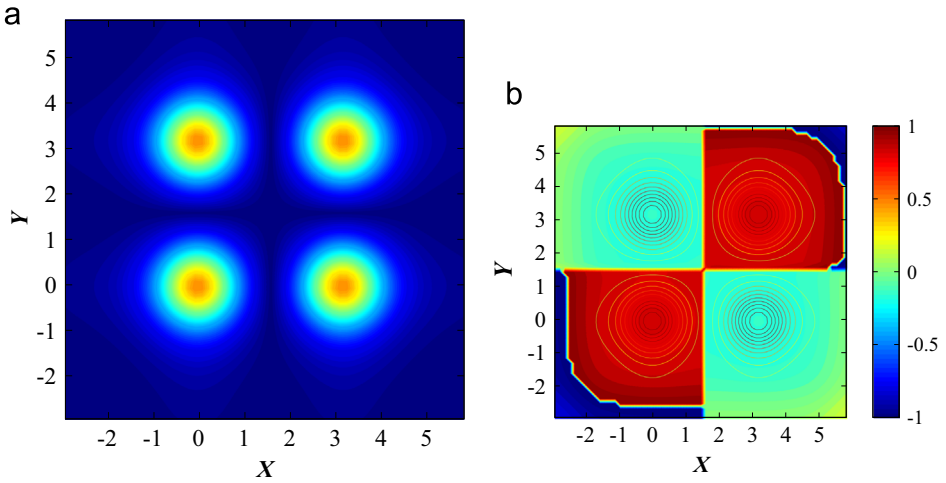


**Fig. 8.** The distribution of the amplitude (a) and phase (in units of $\pi$) in the stable stationary offsite-centered quadrupole used in the simulations. The color code for the amplitude is the same as in Fig. 1(a).

the third moving dipole and six quiescent ones, which brings the total number of solitons to 18, as said above. The total energy increases up to about 24 times the energy of a quiescent soliton, which corresponds to the 12 such solitons, plus the 3 moving dipoles, with the energy of a moving soliton being about twice that of a quiescent one (see Fig. 10(b)). Due to the periodic b.c., the three moving dipoles hit the previously generated quiescent chain, one after the other (see Fig. 10(a)). As a result, two first dipoles are captured by the chain increasing the number of the bound solitons in it, while the third moving dipole is absorbed without adding

new solitons to the chain. This complex interaction results in a chain of 8 quiescent dipoles (equivalent to 16 solitons). The so-generated dipole train originally features intrinsic oscillations, which are eventually damped, see Fig. 10(d). Note that Fig. 10 (a) shows only the constituent fundamental solitons on line $Y=0$, in terms of Fig. 10(c), their counterparts on the line of $Y=3$ showing the same picture.

As mentioned above and shown in Fig. 11, at $k_0 > 2.48$ the initial quadrupole splits into two dipoles, which move at different velocities, without the formation of additional soliton pairs. Each dipole keeps the phase difference of $\pi$ between the constituent solitons.

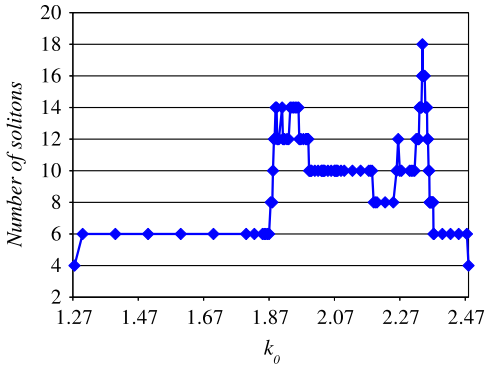


**Fig. 9.** The total number of fundamental solitons in the pattern produced by kick $k_0$ applied to the stable offsite-centered quadrupole. Each dipole counts as two solitons.

## 5. The pattern formation by kicked vortices

### 5.1. Chaotic patterns generated by kicked rhombic (onsite-centered) vortices

It is well known that the lattice potential supports localized vortical modes of two types, the onsite- and offsite-centered ones [26–28]. First, we consider the pattern-formation dynamics for horizontally kicked rhombic vortices built of four fundamental solitons with an empty site in the center, which carry the total phase circulation of $2\pi$, corresponding to the topological charge $S=1$, see Fig. 12(a).

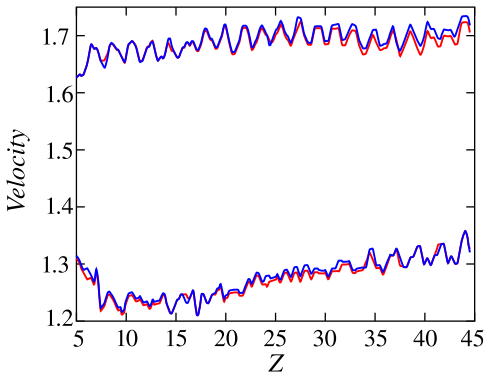


**Fig. 11.** Velocities of two dipoles into which the kicked quadrupole splits at $k_0 = 3$.

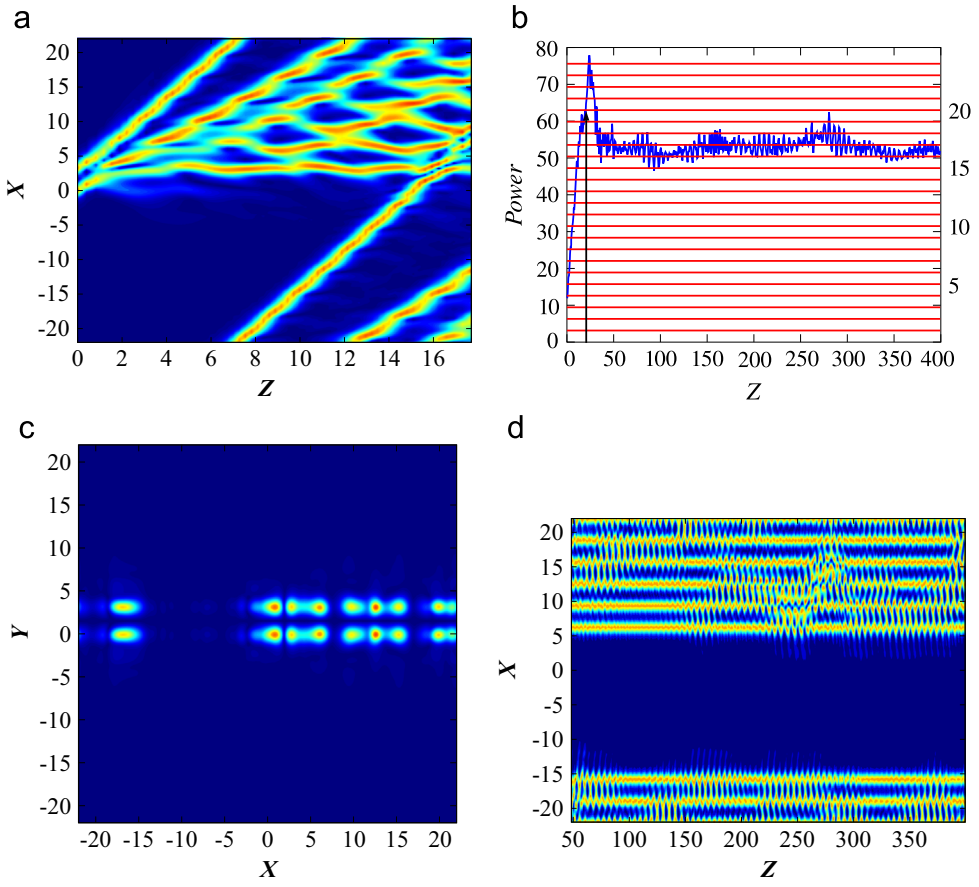


**Fig. 10.** The evolution of the horizontally kicked quadrupole, for $k_0 = 2.339$. (a) Field $|u(X,Y,Z)|$ in the cross section $Y=0$, before the collision of the moving dipole with the pinned complex. (b) The total power versus $Z$ (the vertical arrow indicates the collision point); the horizontal red lines show the power corresponding to $n$ quiescent fundamental solitons, $n$ being the numbers indicated on the right vertical axis. (c) Field $|u(X,Y)|$ at $Z=399.34$. (d) Field $|u(X,Y,Z)|$ in the cross section $Y=0$, after the collision. The color code is the same as in Fig. 1(a). (For interpretation of the references to color in this figure caption, the reader is referred to the web version of this paper.)

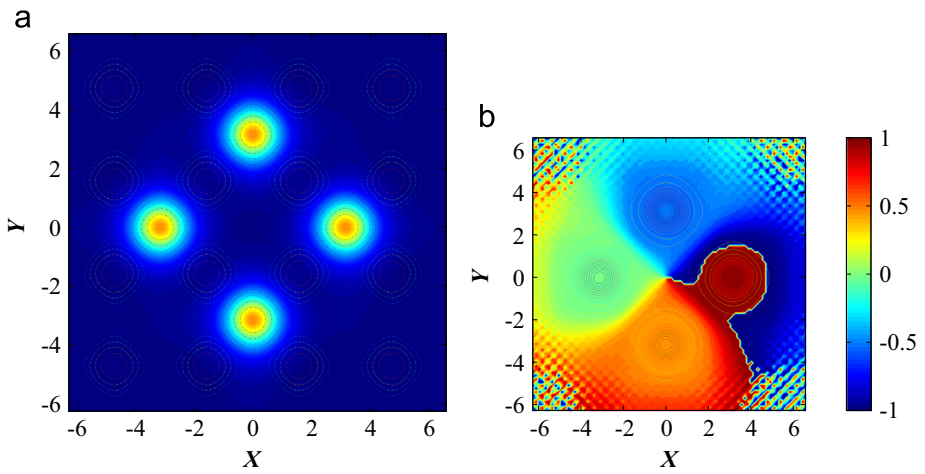


**Fig. 12.** (a, b) The distribution of the amplitude and phase (in units of $\pi$) in the stable onsite-centered (rhombus-shaped) vortex. The lines are level contours of potential $V$. The color code for the amplitude is the same as in Fig. 1(a).

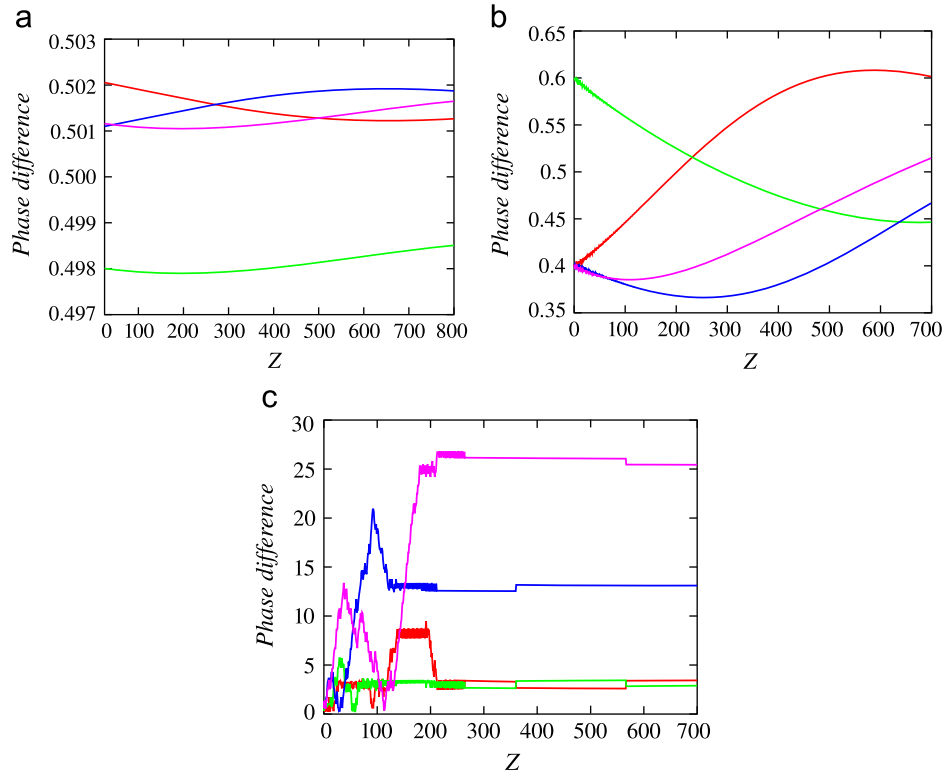


**Fig. 13.** The phase difference between adjacent constituent solitons (in units of $\pi$), versus $Z$, in a weakly kicked rhombic vortex, for different values of the kick's strength: (a) $k_0 = 0$, (b) $k_0 = 0.1$, and (c) $k_0 = 0.2$.

A weak horizontal kick, with $k_0 \lesssim 0.1$, excites oscillations of the constituent fundamental solitons which built the vortex, while vorticity $S=1$ is maintained (i.e., phase differences between the adjacent solitons remain very close to $\pi/2$), see Fig. 13(b). A stronger kick (for instance, $k_0 = 0.5$) destroys the vortical phase structure, and transforms the vortex into a quadrupole, as shown in Fig. 13(c).

At $k_0 = 1.0$ and $k_0 = 1.5$, see Figs. 14 and 15, respectively, the kick completely destroys the vortices, which are replaced by apparently random clusters of quiescent fundamental solitons. Note that, although the results shown in Figs. 14 and 15 have been obtained with absorbing b.c., rather than periodic ones, this circumstance does not affect the results. The same type of b.c. is used below.

### 5.2. Kicked offsite-centered (square-shaped) vortices

Unlike their onsite-centered counterparts, quiescent offsite-centered vortices, such as the one shown in Fig. 16, are unstable in the entire parameter space of Eq. (1) which we have explored, in agreement with the general trend of the offsite-centered vortices to be more fragile than their onsite-centered counterparts [27]. As a result of the instability development, they are transformed into stable quadrupoles. Nevertheless, results displayed below confirm that it is relevant to consider dynamical pattern formation by unstable kicked vortices as this type.

First, we consider the application of the horizontal kick (3) corresponding to $\theta = 0$ and varying strength $k_0$. The fundamental solitons building the vortex oscillate without setting in progressive

motion below the threshold, $k_0 \le k_0^{(\mathrm{thr})} = 1.2125$, cf. Eqs. (5)–(7). Actually, it may happen, in this case, that a new soliton is created and starts moving in the horizontal direction, but the energy is not sufficient to stabilize it, and the new soliton decays eventually, while the initial solitons which compose the offsite-centered vortex are recovered at the original positions. The inner phase structure of the unstable offsite-centered vortices is destroyed in the course of the oscillations, and it transforms into a quadrupole, in accordance with the above-mentioned fact that this is the outcome of its instability in the absence of the kick.

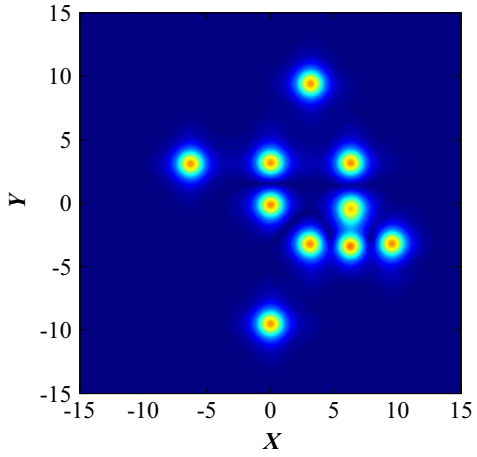


**Fig. 14.** Field $|u(X,Y)|$ at $Z$=299.725, generated by the kicked rhombic vortex for $k_0 = 1.0$. The color code is the same as in Fig. 1(a).

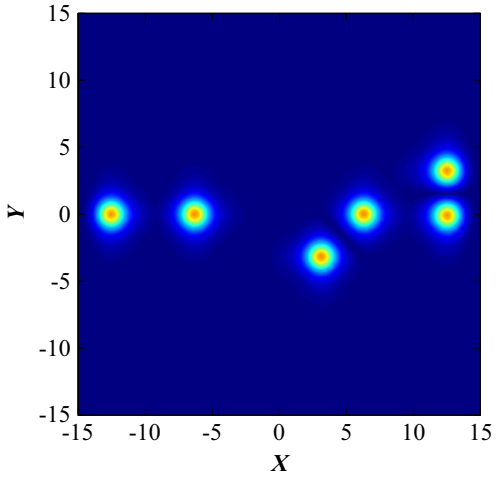


**Fig. 15.** The same as in Fig. 14, but for $k_0 = 1.5$. The color code is the same as in Fig. 1(a).

The increase of $k_0$ leads to the formation of new 2D patterns. At $k_0 = 1.5$, the right vertical pair (column) of the fundamental solitons, which are a part of the original vortical square, start to duplicate themselves, while moving to the right (in the direction of the kick), see Fig. 17. A noteworthy effect is breaking of the symmetry between the top and bottom solitons in the column by the kick, only the bottom soliton succeeding to create a horizontal array of additional solitons (three ones, in total). In this case, Fig. 18 shows that the eventual value of the total power (2) oscillates between values corresponding to the cumulative power of 7 or 8 quiescent fundamental solitons. The resulting pattern develops a disordered form, which oscillates randomly, as Fig. 18 clearly demonstrates.

At somewhat higher values of $k_0$ (for example, $k_0 = 2.0$), the original four-soliton set is transformed into a quiescent three-soliton complex, while an extra dipole and separate free solitons are created and travel through the lattice, see Fig. 19.

Finally, a still stronger kick applied to the square-shaped vortex transforms it into a square-shaped cluster of four solitons moving as a whole, see Figs. 20 and 21, which display the result in the 3D form. In the former case, at $k_0$=2.5, the cluster leaves behind a copy of one of the original solitons, while at $k_0$=3.0 the moving cluster is the single emerging mode. Although the clusters are dynamically stable, they do not carry the vortical phase structure.

We have also studied the application of the kick to the offsite-centered vortex in other directions, i.e., varying angle $\theta$ in Eq. (4). First, as seen in Fig. 22(a), in the case of $\theta = \pi/8$ and $k_0 = 1.5$, the kick again breaks the symmetry between the top and bottom rows of the solitons, generating an array of additional solitons in the bottom horizontal row. Further, to check that the numerical code is compatible with the global symmetry of the setting, we also considered equivalent angles, $\theta = 5\pi/8$, $9\pi/8$ and $13\pi/8$. The results, shown in Fig. 22, evidence the possibility of controlling the direction of the emission of the soliton array by the direction of the initial kick.

Further, running the computations for varying $\theta$ and moderate values of $k_0$, we have concluded that there is a threshold angle $\varepsilon$, so that the emission towards any of the four equivalent directions,

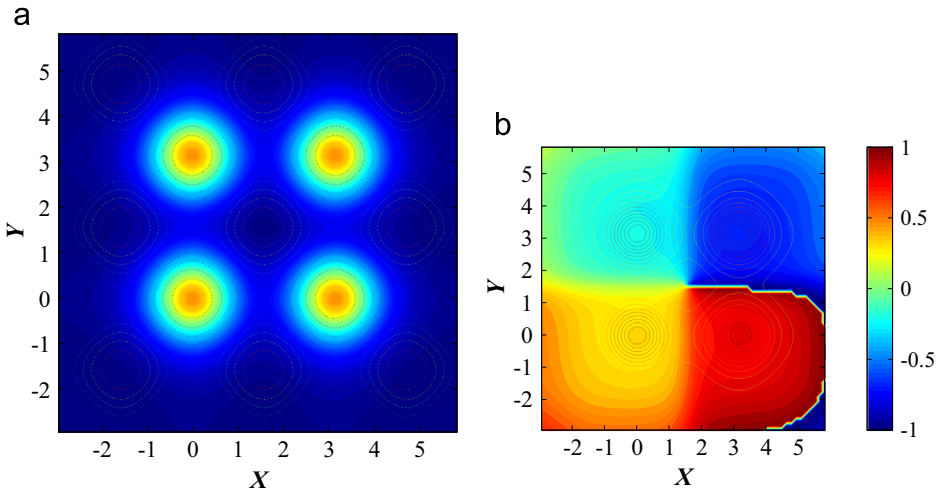


**Fig. 16.** The distribution of the amplitude (a) and phase (b) in the unstable offsite-centered vortex. The lines are level contours of potential $V$. The color code for the amplitude is the same as in Fig. 1(a).

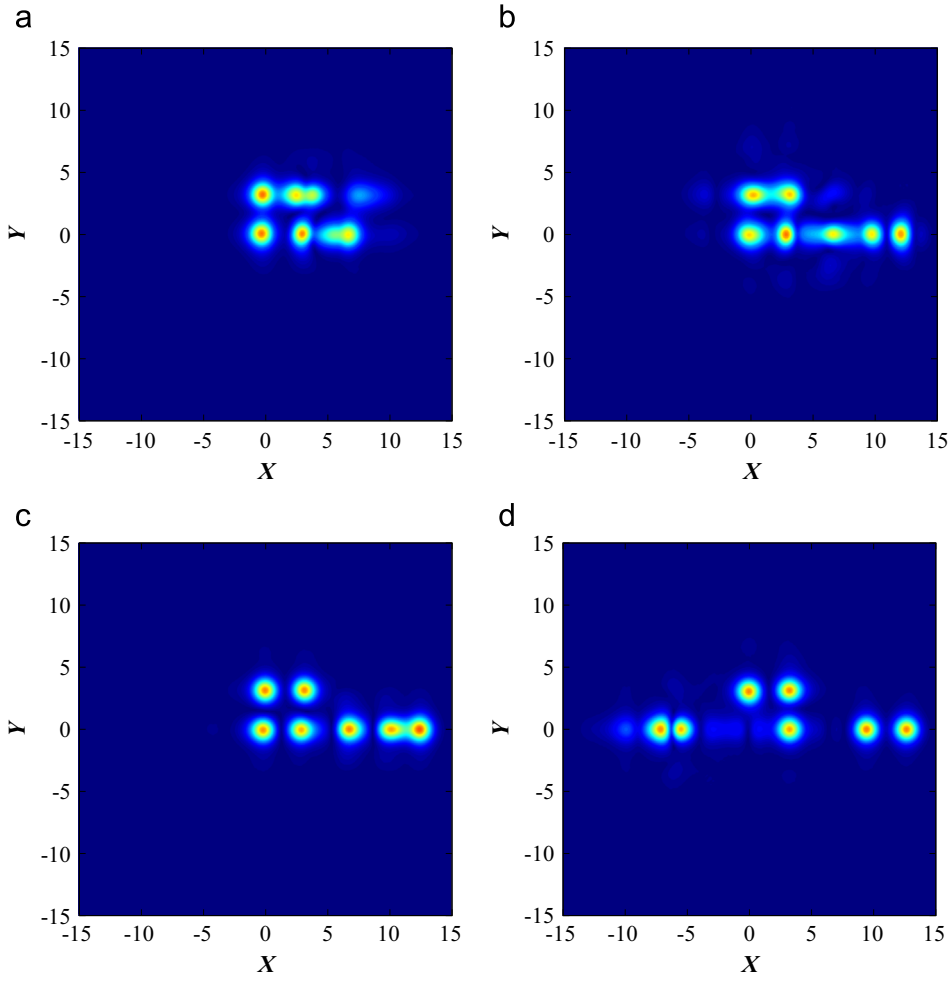


**Fig. 17.** The evolution of the unstable offsite-centered vortex kicked in the horizontal direction ($\theta = 0$) with $k_0 = 1.5$. The color code is the same as in Fig. 1(a). (a) $Z = 2.6593$, (b) $Z = 12.008$, (c) $Z = 239.91$, and (d) $Z = 299.825$.

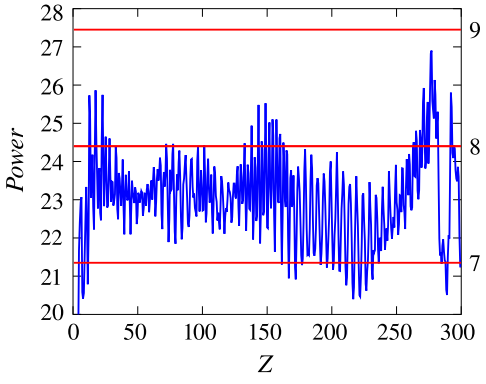


**Fig. 18.** The evolution of the total power for the pattern produced by horizontally kicking the offsite-centered vortex, for $k_0 = 1.5$. The red horizontal lines show power levels corresponding to $n$ quiescent solitons. (For interpretation of the references to color in this figure caption, the reader is referred to the web version of this paper.)

corresponding to directions $\phi = 0, \pi/2, \pi$ or $3\pi/2$, occurs provided that the orientation of the kick belongs to a certain range around this direction, viz., $(\phi - \pi/4 + \varepsilon) < \theta < (\phi + \pi/4 - \varepsilon)$, with $\varepsilon = 0.059$. If the kick's orientation falls into interstices between these ranges, namely $[\phi + \pi/4 - \varepsilon; \phi + \pi/4 + \varepsilon]$, solitons arrays are not generated. In the latter case, the square vortex transforms into a quadrupole.

These results can be explained by noting that the intrinsic phase circulation in the vortex is directed counterclockwise (from $X$ to $Y$). Then, as schematically shown (for example) for $\theta = \pi/8$ in Fig. 23, the superposition of the externally applied kick (the phase gradient) and the intrinsic phase flow gives rise to the largest local phase gradient at the position of the bottom right soliton, in the positive horizontal direction, therefore the array is emitted accordingly.

It is also instructive to perform the simulations for the vortex with the opposite vorticity ($-1$ instead of $+1$). In this way, the expected symmetry reversal has been verified (not shown here in detail): The same results as above are obtained, with angle $\theta$ replaced by its counterpart, which is symmetric with respect to the closest coordinate axis. We also note that identical results were obtained using both periodic and absorbing boundary conditions.

## 6. Conclusions

The objective of this work is to extend the analysis of the dynamical pattern-formation scenarios in the CQ-CGL (cubic–quintic complex Ginzburg–Landau) equation with the 2D cellular potential. The equation is the model for laser cavities with built-in gratings, represented by the spatially periodic potential. Recently, the quasi-1D pattern-formation scenarios, initiated by the moving fundamental solitons, were studied in this model. Here, we have

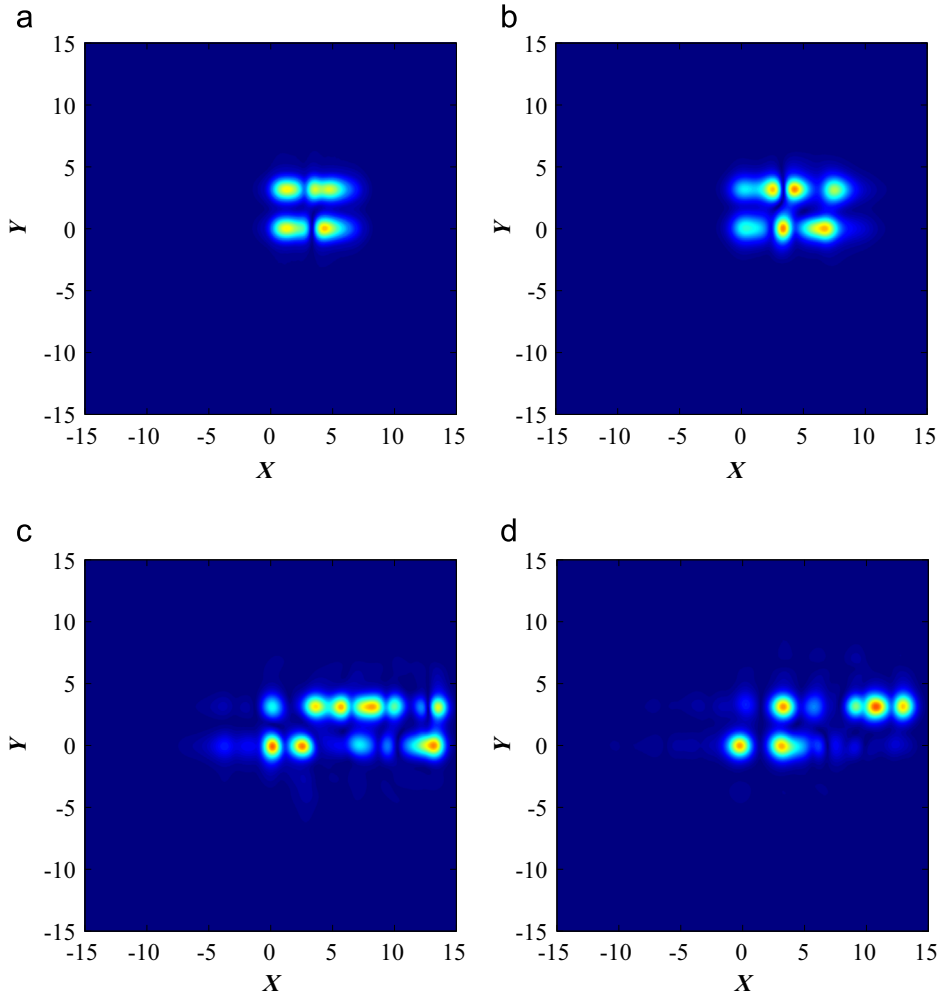


**Fig. 19.** The evolution pattern produced by horizontally kicking the offsite-centered vortex, for $k_0 = 2$. The color code is the same as in Fig. 1(a). (a) $Z=1.0784$, (b) $Z=2.0680$, (c) $Z=5.1432$, and (d) $Z=7.5069$.

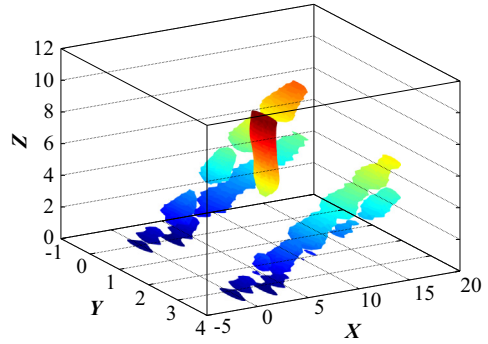


**Fig. 20.** The three-dimensional rendition of the evolution of the horizontally kicked offsite-centered vortex for $k_0 = 2.5$, which is transformed into a stably moving four-soliton cluster. The chromatic progression indicates the propagation direction. The vertical rod represents the additional quiescent fundamental soliton, left in the wake of the moving four-soliton cluster.

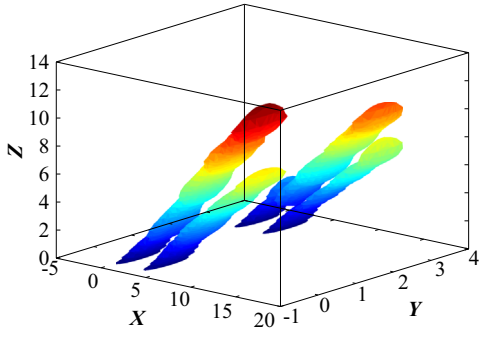


**Fig. 21.** The same as in Fig. 20 but for $k_0 = 3.0$. In this case, the unstable vortex is entirely transformed into the stable moving cluster.

systematically analyzed the fully 2D scenarios, produced by kicking compound modes, viz., dipoles, offsite-centered quadrupoles, and vortices of two different types, onsite- and offsite-centered ones. The motion of the kicked compound through the cellular potential leads to the generation of diverse multi-peak patterns pinned to the lattice, which the moving object leaves in its wake. In the annular system with periodic boundary conditions, the persistently traveling dipole hits the pinned pattern from the opposite direction. In this way, several dynamical regimes are initiated, including the periodically recurring elastic passage of the free dipole through the quiescent one, and transient regimes, which lead, after a few quasi-elastic collisions, to absorption of one dipole by the other. In the case of vortices, the dependence of the outcome on the magnitude and direction of the kick was also investigated. In particular, a noteworthy result is that a strong kick transforms the original offsite-centered vortex (which is unstable by itself) into a clean stably moving four-soliton cluster.

The analysis can be extended by considering two-component systems (which would take the polarization of light into account),

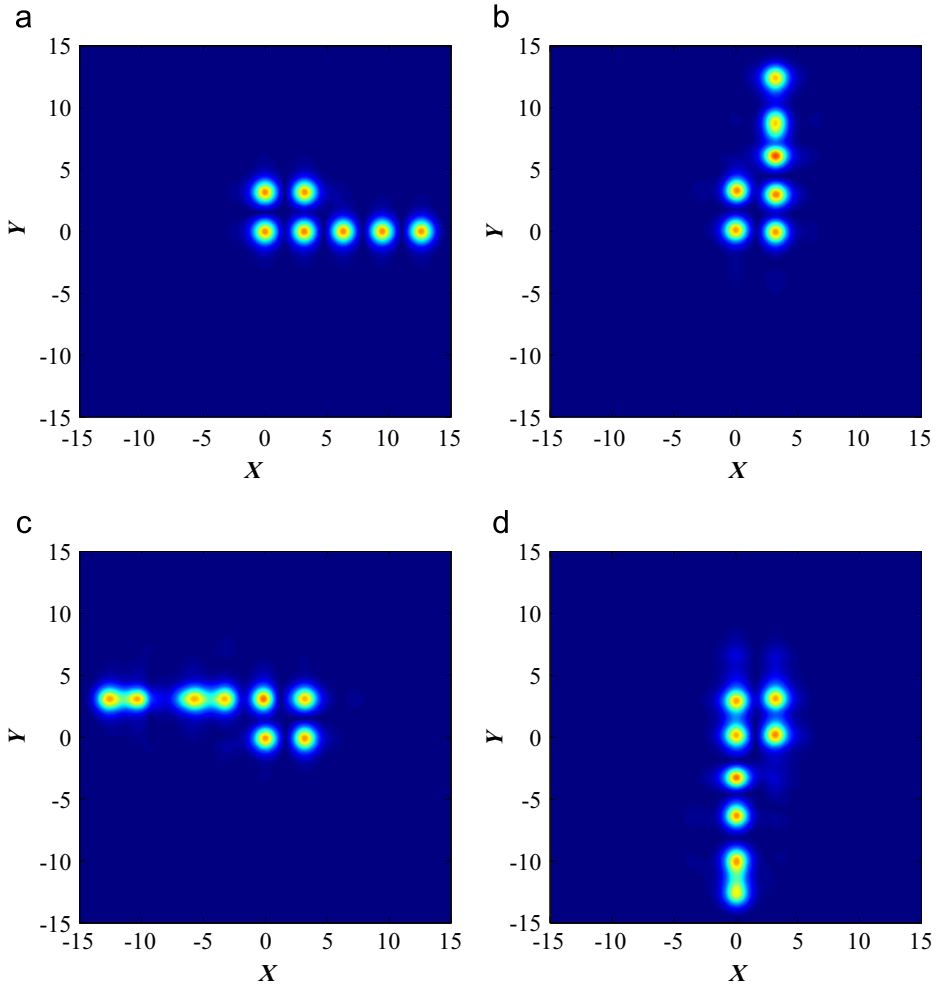


**Fig. 22.** The pattern produced by the offsite-centered vortex kicked with strength $k_0 = 1.5$ in different but actually equivalent directions: (a) $\theta = \pi/8$, (b) $\theta = 5\pi/8$, (c) $\theta = 9\pi/8$, and (d) $\theta = 13\pi/8$. The color code is the same as in Fig. 1(a).

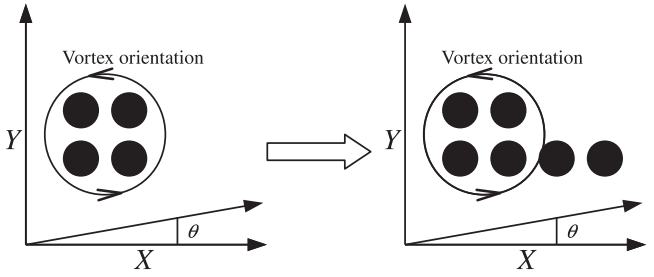


**Fig. 23.** The explanation of the direction in which the soliton array is emitted from the kicked offsite-centered vortex.

collisions between independently created moving modes, and the motion of kicked solitons in inhomogeneous lattices. Eventually, the analysis may be generalized for the three-dimensional setting, which is not relevant to optics, but may be realized, in principle, in terms of Bose–Einstein condensates of polariton–exciton quasi-particles [29].

## Acknowledgements

The work of DM was supported in part by a Senior Chair Grant from the Région Pays de Loire, France. Support from the Romanian Ministry of Education and Research (Project PN-II-ID-PCE-2011-3-0083) is also acknowledged by this author.

## References

[1] N. Akhmediev, A. Ankiewicz (Eds.), Dissipative Solitons, Lecture Notes in Physics, vol. 661, Springer, Berlin, 2005;
N. Akhmediev, A. Ankiewicz (Eds.), Dissipative Solitons: From Optics to Biology and Medicine, Lecture Notes in Physics, vol. 751, Springer, Berlin, 2008.
[2] N.N. Rosanov, Spatial Hysteresis and Optical Patterns, Springer, Berlin, 2002.
[3] S. Barland, J.R. Tredicce, M. Brambilla, L.A. Lugiato, S. Balle, M. Giudici, T. Maggipinto, L. Spinelli, G. Tissoni, T. Knödl, M. Miller, R. Jäger, Nature (London) 419 (2002) 699;
Z. Bakonyi, D. Michaelis, U. Peschel, G. Onishchukov, F. Lederer, J. Opt. Soc. Am. B 19 (2002) 487;
E.A. Ultanir, G.I. Stegeman, D. Michaelis, C.H. Lange, F. Lederer, Phys. Rev. Lett. 90 (2003) 253903;
P. Mandel, M. Tlidi, J. Opt. B: Quantum Semiclassical. Opt. 6 (2004) R60;
N.N. Rosanov, S.V. Fedorov, A.N. Shatsev, Appl. Phys. B 81 (2005) 937;
C.O. Weiss, Ye. Larionova, Rep. Prog. Phys. 70 (2007) 255;
N. Veretenov, M. Tlidi, Phys. Rev. A 80 (2009) 023822;
M. Tlidi, A.G. Vladimirov, D. Pieroux, D. Turaev, Phys. Rev. Lett. 103 (2009) 103904;
P. Genevet, S. Barland, M. Giudici, J.R. Tredicce, Phys. Rev. Lett. 104 (2010) 223902;
P. Grelu, N. Akhmediev, Nat. Photonics 6 (2012) 84;
J. Jiménez, Y. Noblet, P.V. Paulau, D. Gomila, T. Ackemann, J. Opt. 15 (2013) 044011;
C. Fernandez-Oto, M.G. Clerc, D. Escaff, M. Tlidi, Phys. Rev. Lett. 110 (2013) 174101.
[4] N. Lazarides, G.P. Tsironis, Phys. Rev. E 71 (2005) 036614;
Y.M. Liu, G. Bartal, D.A. Genov, X. Zhang, Phys. Rev. Lett. 99 (2007) 153901;
E. Feigenbaum, M. Orenstein, Opt. Lett. 32 (2007) 674;
I.R. Gabitov, A.O. Korotkevich, A.I. Maimistov, J.B. Mcmahon, Appl. Phys. A 89 (2007) 277;
A.R. Davoyan, I.V. Shadrivov, Y.S. Kivshar, Opt. Exp. 17 (2009) 21732;
K.Y. Bliokh, Y.P. Bliokh, A. Ferrando, Phys. Rev. A 79 (2009) 041803;

E.V. Kazantseva, A.I. Maimistov, Phys. Rev. A 79 (2009) 033812;
Y.-Y. Lin, R.-K. Lee, Y.S. Kivshar, Opt. Lett. 34 (2009) 2982;
A. Marini, D.V. Skryabin, Opt. Lett. 81 (2010) 033850;
A. Marini, D.V. Skryabin, B.A. Malomed, Opt. Exp. 19 (2011) 6616.
[5] V.I. Petviashvili, A.M. Sergeev, Dokl. AN SSSR 276 (1984) 1380 [Sov. Phys. Doklady 29, 493 (1984)].
[6] I.S. Aranson, L. Kramer, Rev. Mod. Phys. 74 (2002) 99;
B.A. Malomed, in: A. Scott (Ed.), Encyclopedia of Nonlinear Science, Routledge, New York, 2005, p. 157.
[7] J. Anglin, Phys. Rev. Lett. 79 (1997);
F.T. Arecchi, J. Bragard, L.M. Castellano, Opt. Commun. 179 (2000) 149;
J. Keeling, N.G. Berloff, Phys. Rev. Lett. 100 (2008) 250401;
B.A. Malomed, O. Dzyapko, V.E. Demidov, S.O. Demokritov, Phys. Rev. B 81 (2010) 024418.
[8] M.C. Cross, P.C. Hohenberg, Rev. Mod. Phys. 65 (1993) 851.
[9] K.-H. Hoffmann, Q. Tang, Ginzburg–Landau Phase Transition Theory and Superconductivity, Birkhauser Verlag, Basel, 2001.
[10] B.A. Malomed, Physica D 29 (1987) 155.
[11] O. Thual, S. Fauve, J. Phys. (Paris) 49 (1988) 1829;
S. Fauve, O. Thual, Phys. Rev. Lett. 64 (1990) 282;
W. van Saarloos, P.C. Hohenberg, Phys. Rev. Lett. 64 (1990) 749;
V. Hakim, P. Jakobsen, Y. Pomeau, Europhys. Lett. 11 (1990) 19;
B.A. Malomed, A.A. Nepomnyashchy, Phys. Rev. A 42 (1990) 6009;
P. Marcq, H. Chaté, R. Conte, Physica D 73 (1994) 305;
N. Akhmediev, V.V. Afanasjev, Phys. Rev. Lett. 75 (1995) 2320;
H.R. Brand, R.J. Deissler, Phys. Rev. Lett. 63 (1989) 2801;
V.V. Afanasjev, N. Akhmediev, J.M. Soto-Crespo, Phys. Rev. E 53 (1996) 1931;
J.M. Soto-Crespo, N. Akhmediev, A. Ankiewicz, Phys. Rev. Lett. 85 (2000) 2937;
H. Leblond, A. Komarov, M. Salhi, A. Haboucha, F. Sanchez, J. Opt. A: Pure Appl. Opt. 8 (2006) 319;
W.H. Renninger, A. Chong, F.W. Wise, Phys. Rev. A 77 (2008) 023814;
J.M. Soto-Crespo, N. Akhmediev, C. Mejia-Cortes, N. Devine, Opt. Express 17 (2009) 4236;
D. Mihalache, Proc. Romanian Acad. A 11 (2010) 142;
Y.J. He, B.A. Malomed, D. Mihalache, F.W. Ye, B.B. Hu, J. Opt. Soc. Am. B 27 (2010) 1266;
D. Mihalache, Romanian Rep. Phys. 63 (2011) 325;
C. Mejia-Cortes, J.M. Soto-Crespo, R.A. Vicencio, M.I. Molina, Phys. Rev. A 83 (2011) 043837;
D. Mihalache, Romanian J. Phys. 57 (2012) 352;
O.V. Borovkova, V.E. Lobanov, Y.V. Kartashov, L. Torner, Phys. Rev. A 85 (2012) 023814.
[12] L.-C. Crasovan, B.A. Malomed, D. Mihalache, Phys. Rev. E 63 (2001) 016605;
L.-C. Crasovan, B.A. Malomed, D. Mihalache, Phys. Lett. A 289 (2001) 59;
D. Mihalache, D. Mazilu, F. Lederer, Y.V. Kartashov, L.-C. Crasovan, L. Torner, B. A. Malomed, Phys. Rev. Lett. 97 (2006) 073904;
D. Mihalache, D. Mazilu, F. Lederer, H. Leblond, B.A. Malomed, Phys. Rev. A 76 (2007) 045803;
D. Mihalache, D. Mazilu, F. Lederer, H. Leblond, B.A. Malomed, Phys. Rev. A 75 (2007) 033811;
D. Mihalache, D. Mazilu, Romanian Rep. Phys. 60 (2008) 749.
[13] M. Tlidi, M. Haelterman, P. Mandel, Europhys. Lett. 42 (1998) 505;
M. Tlidi, P. Mandel, Phys. Rev. Lett. 83 (1999) 4995;
M. Tlidi, J. Opt. B: Quantum Semiclassical Opt. 2 (2000) 438.
[14] H. Sakaguchi, Physica D 210 (2005) 138.
[15] V. Skarka, N.B. Aleksić, Phys. Rev. Lett. 96 (2006) 013903;
N.B. Aleksić, V. Skarka, D.V. Timotijević, D. Gauthier, Phys. Rev. A 75 (2007) 061802;
V. Skarka, D.V. Timotijević, N.B. Aleksić, J. Opt. A: Pure Appl. Opt. 10 (2008) 075102;
V. Skarka, N.B. Aleksić, H. Leblond, B.A. Malomed, D. Mihalache, Phys. Rev. Lett. 105 (2010) 213901.
[16] A. Szameit, J. Burghoff, T. Pertsch, S. Nolte, A. Tünnermann, Opt. Express 14 (2006) 6055.
[17] J.W. Fleischer, M. Segev, N.K. Efremidis, D.N. Christodoulides, Nature 422 (2003) 147.
[18] H. Leblond, B.A. Malomed, D. Mihalache, Phys. Rev. A 80 (2009) 033835.
[19] M. Tlidi, Paul Mandel, R. Lefever, Phys. Rev. Lett. 73 (1994) 640.
[20] W.J. Firth, A.J. Scroggie, Phys. Rev. Lett. 76 (1996) 1623.
[21] M. Brambilla, A. Gatti, L.A. Lugiato, Adv. At. Mol. Opt. Phys. 40 (1998) 229.
[22] S.V. Fedorov, A.G. Vladimirov, G.V. Khodova, N.N. Rosanov, Phys. Rev. E 61 (2000) 5814.
[23] D. Mihalache, D. Mazilu, V. Skarka, B.A. Malomed, H. Leblond, N.B. Aleksić, F. Lederer, Phys. Rev. A 82 (2010) 023813.
[24] D. Mihalache, D. Mazilu, F. Lederer, H. Leblond, B.A. Malomed, Phys. Rev. A 81 (2010) 025801.
[25] V. Besse, H. Leblond, D. Mihalache, B.A. Malomed, Phys. Rev. E 87 (2013) 012916.
[26] B.B. Baizakov, B.A. Malomed, M. Salerno, Europhys. Lett. 63 (2003) 642;
J. Yang, Z.H. Musslimani, Opt. Lett. 28 (2003) 2094.
[27] T. Mayteevarunyoo, B.A. Malomed, B.B. Baizakov, M. Salerno, Physica D 238 (2009) 1439.
[28] J. Yang, Nonlinear Waves in Integrable and Nonintegrable Systems, SIAM, Philadelphia, 2010.
[29] H. Deng, H. Haug, Y. Yamamoto, Rev. Mod. Phys. 82 (2010) 1489;
B. Deveaud-Plédran, J. Opt. Soc. Am. B 29 (2012) A138;
N.G. Berloff, J. Keeling, in: A. Bramati, M. Modugno (Eds.), Universality in Modelling Non-Equilibrium Pattern Formation in Polariton Condensates, Physics of Quantum Fluids, Springer, Berlin, Heidelberg, 2013, pp. 19–38.